A molecular understanding of magnesium aluminium silicate – drug, drug - polymer, magnesium aluminium silicate - polymer nanocomposite complex interactions in modulating drug release: Towards zero order release

A.M. Totea[1], I. Dorin[2], P.R. Laity[3], Juan Sabin[4], B.R. Conway[1], L. Waters[1], K. Asare-Addo[1*]

[1]School of Applied Sciences, Department of Pharmacy, University of Huddersfield, Queensgate, Huddersfield, UK, HD1 3DH

[2]Biomolecular Formulation and Characterization Sciences, UCB, Slough, SL3WE, UK

[3]Department of Materials Science and Engineering, University of Sheffield, Sir Robert Hadfield Building, Mappin Street, Sheffield, S1 3JD, UK

[4]AFFINImeter, Edificio Emprendia, Campus Vida, Santiago de Compostela, Spain

*Corresponding author (Kofi Asare-Addo)

e-mail: k.asare-addo@hud.ac.uk

Tel: +44 1484 472360

Fax: +44 1484 472182

Submission: EJPB

Graphical abstract

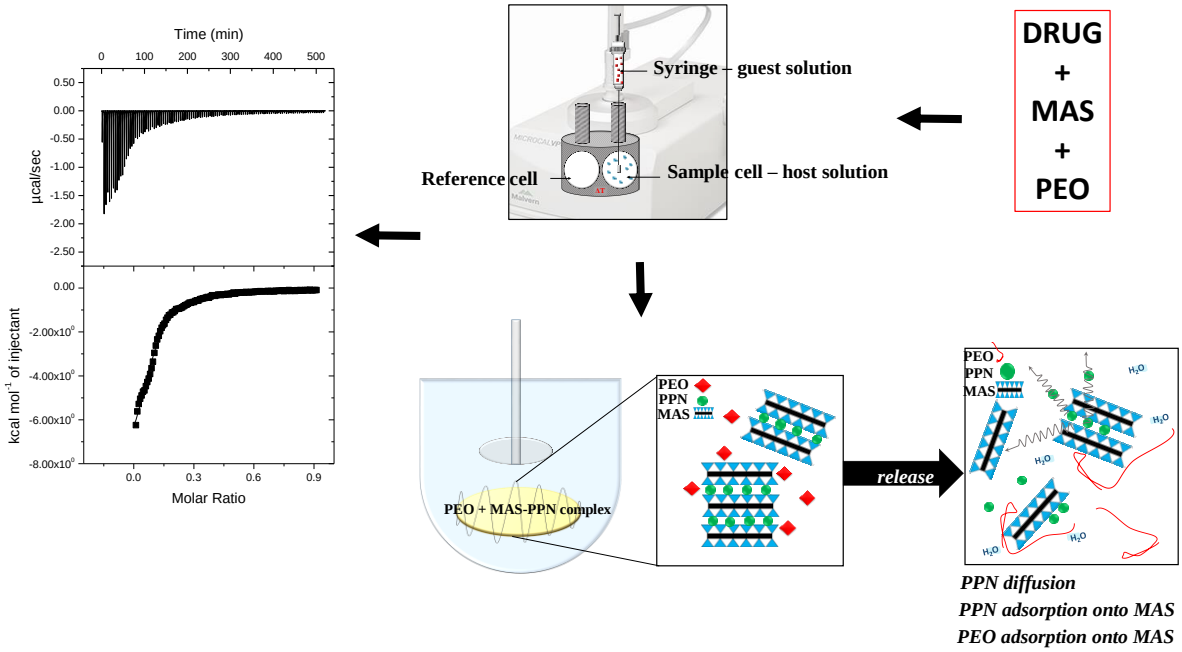

Highlights

MAS-PPN complexes fully characterized up to nanometer scale

MAS-PPN, MAS-PEO and PPN-MAS-PEO complexation extensively studied using ITC

Thermodynamics at molecular level suggests binding process was enthalpy driven and entropically unfavourable

Compacts from complexes showed reduced elasticity

Controlled release of PPN observed at significantly low polymer levels (5 %)

Zero-order release achieved for MAS-PPN complexes at 50% polymer level in acid and buffer media

Abstract

This study reports the use of ITC in understanding the thermodynamics occurring for a controlled release system in which complexation has been exploited. In this study, a model drug, propranolol hydrochloride (PPN) was complexed with magnesium aluminium silicate (MAS) and these complexes were used in combination with polyethylene oxide (PEO) as a hydrophilic carrier at various concentrations to sustain the release of PPN. DSC, XRPD, ATR-FTIR and SEM/EDX were successfully used in characterising the produced complexes. 2D-SAXS data patterns for MAS and the produced complexes were shown to be symmetric and circular with the particles showing no preferred orientation at the nanometre scale. ITC studies showed differences between PPN adsorption onto MAS compared with PPN adsorption onto a MAS-PEO mixture. At both temperatures studied the binding affinity K_a was greater for the titration of PPN into the MAS-PEO mixture (5.37E+04 ± 7.54E+03 M at 25 °C and 8.63E+04 ± 6.11E+03 M at 37 °C), compared to the affinity obtained upon binding between PPN and MAS as previously reported suggesting a stronger binding with implications for the dissolution process. MAS-PPN complexes with the PEO polymer compacts displayed desired manufacturing and formulation properties for a formulator including, reduced plastic recovery therefore potentially reducing the risk of cracking/splitting and on tooling wear, controlled release of PPN at a significantly low (5 %) polymer level as well as a zero-order release profile (case II transport) using up to 50 % polymer level.

Keywords: magnesium aluminium silicate, propranolol hydrochloride, isothermal titration calorimetry, complexation, small angle X-ray scattering

Abbreviations: MAS, magnesium aluminium silicate; PPN, propranolol hydrochloride; ITC, isothermal titration calorimetry; SIM, single injection mode; MIM, multiple injection mode;

HPLC, high performance liquid chromatography; RSD, relative standard deviation; ICH, International Conference on Harmonisation; LOD, limit of detection; LOQ, limit of quantification; HCl, hydrochloric acid; rpm, rotations per minute; MDT, mean dissolution time; MDR, mean dissolution rate

1. Introduction

Minerals are widely used in the pharmaceutical industry and in medicine (Gomes, 2018). Minerals are easily available in nature and are used for their nutritional, cosmetic and therapeutic properties due to their safety and physicochemical properties. Novel practices involve the use of minerals as drug carriers in the formulation of pharmaceutical dosage forms through their capacity to adsorb or reversibly fixate polar compounds onto their structure and form complex dispersions and particles (Carretero and Pozo, 2009). Magnesium aluminium silicate (MAS) is the mineral of interest in this research study. MAS is a mixture of natural smectite montmorillonite and saponite clays which is non-toxic nor irritant. These desirable qualities lends itself for use within drug formulation. MAS has a high surface area with a very good affinity with cationic drugs and polymers such as chitosan and quaternary polymethacrylate (Khlibsuwan and Ponjanyakul, 2016, 2018; Khlibsuwan et al, 2017; Rongthong et al., 2013; 2015). MAS has also been used to improve the physical characteristics of drugs and to control their release (Pongjanyakul, Khunawattanakul and Puttipipatkhachorn, 2009; Kanjanakawinkul *et al.*, 2013). Several authors have used MAS in various applications such as generating microcomposite films for modified release tablets, generating reinforced alginate beads, minimising sticking in Eudragit RL-based films, wafers, mucosal and buccal delivery (Pongjanyakul et al., 2005; Puttipipatkhachorn et al., 2005; Rongthong et al., 2020; Kanjanakawinkul et al., 2013; Pongjanyakul 2013; Adebisi et al., 2015; Okeke and Boateng,

2016, 2017). The layered silicate structure of MAS (Figure 1a) is formed of one alumina or magnesia octahedral sheet, sandwiched between two tetrahedral silicate sheets (Kanjanakawinkul *et al.*, 2013). The complexes formed as a result of the fixation of polar compounds can modify the release of drugs upon administration, which is desirable for drugs having a short half-life and require frequent administration to maintain adequate drug plasma levels that are used to treat chronic conditions (Rojtanatanya and Pongjanyakul, 2010).

Propranolol hydrochloride (PPN) (Figure 1b) used to treat angina pectoris, myocardial infarction and high blood pressure is an antagonist at the β-adrenergic receptors of the heart (β-blockers) (Patrick, 2001; Rojtanatanya and Pongjanyakul, 2010) and is the model drug of choice in the study to form complexes with MAS as it has a short half-life of 3.9 h and therefore needs to be administered frequently (2-3 times/day) in order to maintain adequate drug plasma levels (Datta, 2013). The physicochemical characteristics of the formed complexes are not entirely understood and therefore understanding them is essential to establishing a successful formulation. Recently, Totea et al. exploited isothermal calorimetry in understanding the binding process of MAS to diltiazem hydrochloride and propranolol hydrochloride (Totea et al., 2019, 2020). The authors utilised ITC in understanding the thermodynamics of the binding process. ITC is a powerful and well-established biophysical technique that allows the complete characterisation of the thermodynamics of an interaction in just a single experiment (MicroCal, 1998). The technique measures the formation and dissociation of molecular complexes (Ladbury and Chowdhry, 1996; Penn and Warren, 2009; Le *et al.*, 2013) and as such is suitable in understanding the formed complexes in this study. Callies and Hernández Daranas, 2016 have reported the use of ITC to provide accurate and important information about the mechanisms of binding of molecules (Callies and Hernández Daranas, 2016). From the resulting data, binding site size, affinity (K_a), changes in enthalpy (ΔH), entropy (ΔS), Gibbs free energy (ΔG) and stoichiometry (N) of the binding events can be determined through the

fitting of independent binding sites, sequential binding sites, competitive binding and dissociation models (Moore *et al.*, 2016). For a simple single binding site model, the non-linear least squares fit of the data can be used to determine K_a and ΔH, followed by the calculation of ΔG and ΔS using the known relationship between the van't Hoff equation and change in Gibbs free energy:

$$\Delta G = \Delta H - T\Delta S \qquad \text{Equation 1}$$

$$= -RTlnK_a \qquad \text{Equation 2}$$

where T is the absolute temperature in Kelvin and R is the gas constant.

ΔC_p is determined from the temperature dependence of ΔH using Equation 3 (MicroCal, 1998; Le *et al.*, 2013):

$$\Delta C_p = \frac{(\Delta H_{T2} - \Delta H_{T1})}{T_2 - T_1} \qquad \text{Equation 3}$$

The purpose of the presented research was therefore to understand the process of adsorption of such a drug on MAS and the effects of this process on extending the release of such drugs. Furthermore a hydrophilic polymer, polyethylene oxide (PEO) (Figure 1c) is used in combination with the formulated clay-drug complexes in an attempt to extend drug release. Polymers are of high importance to the pharmaceutical industry as they offer a wide variety of physical and chemical characteristics which can be easily manipulated and are extensively used in the formulation of tablets as to improve bioavailability and control drug release (Sinko, 2010). The ability to extend drug release is also essential in improving patient compliance, hence the popularity of polymers and the rapid advances in the pharmaceutical industry since their introduction. Potential complexations of the complexes is explored to explain observations from the dissolution process at the molecular level. The use of polymers in combination with clay-drug complex particles in the present study offers an in-depth

understanding of controlling drug release using a combined system consisting of a natural drug carrier in a polymeric matrix.

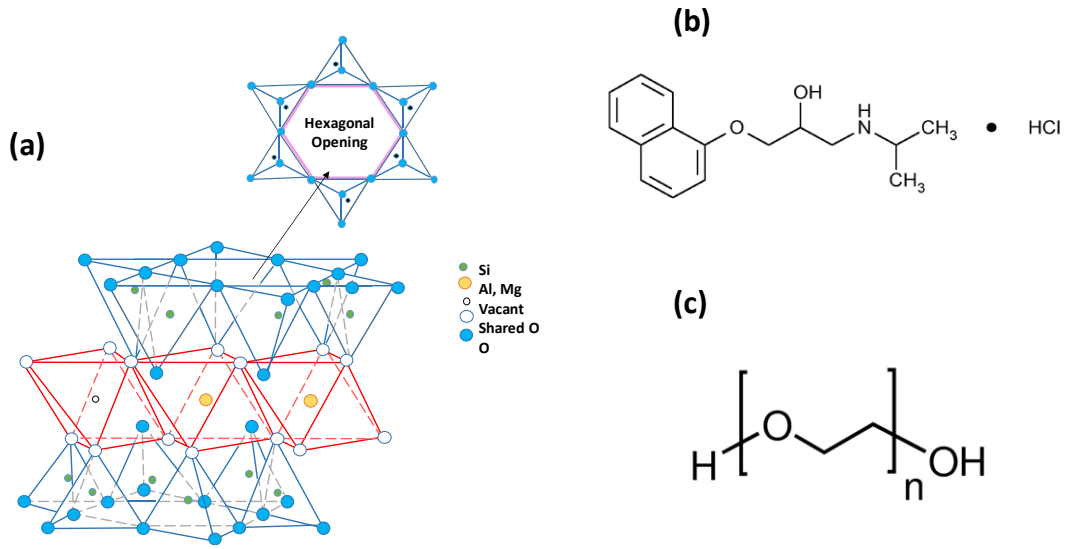

Figure 1. Chemical structures of materials used (a) Alumina or magnesia sheet composed of octahedron structures joined together and sandwiched between two silica sheets composed of silica tetrahedron structures joined together (adapted from (Vanderbilt Minerals, 2014b)), (b) propranolol hydrochloride, (c) polyethylene oxide (PEO).

2. Experimental

2.1. Materials

Veegum F EP® or Magnesium Aluminium Silicate (MAS) was a kind gift from R.T.Vanderbilt Company, Norwalk, CT (USA). Its composition was confirmed as previously reported by Totea et al., 2019. The authors confirmed the material complied with the European Pharmacopoeia monograph for MAS and is indicated for use as a dry excipient in pressed powders and in direct compression tablets (Vanderbilt Minerals, 2014a). Propranolol hydrochloride (PPN) was purchased from TCI (Tokyo Chemical Industry, Tokyo). Polyethylene oxide (PEO, Polyox WSR 301) MW 4,000,000 was a kind gift from Colorcon, UK.

Acetonitrile (HPLC grade), sodium phosphate dibasic dihydrate, 99+ % (HPLC grade), sodium hydroxide and 2 M hydrochloric acid were purchased from Fisher Scientific (UK).

2.2. Methods

2.2.1. Formulation of MAS-PPN complex particles

The methodology of Totea et al. 2019 was used in the formulation of MAS-PPN complex dispersions and particles. A 2 % w/v MAS dispersion and PPN solution were separately prepared under continuous stirring for 24 h, (25 ºC and 500 rpm). A 2 M HCl or 2 M NaOH was used to further adjust the pH of the MAS and PPN to pH 5. For the initial drug loading, MAS dispersion was combined with the PPN solution prepared (1:1 w/w), and the obtained flocculated mixture was incubated at 37 °C with shaking for 24 h. The complex dispersion obtained was then filtered using a Buchner filtration apparatus with vacuum and further transferred into a clean beaker.

For the second drug loading, the collected complexes following filtration were redispersed into a fresh drug solution and incubated at 37 °C with shaking for 24 h. The flocculated complexes obtained were then filtered and dried in the oven at 50 ºC for 48 h. The double loaded MAS–PPN complex dispersions obtained from the drying process were milled (Retsch® PM 100 Ball Mill set at 350 rpm) and the particle size fraction of 65 –123 µm stored in a glass vial and used as needed.

2.2.2. Characterisation of MAS-PPN complexes

2.2.2.1. Attenuated total reflectance Fourier transform infrared spectroscopy (ATR-FTIR)

ATR-FTIR (Smart Orbit ATR-FTIR) was used to characterise potential molecular interactions between MAS and PPN using diamond as the ATR crystal scanned from 4000 to 400 cm^{-1}.

2.2.2.2. Scanning electron microscopy/ energy dispersive X-ray spectroscopy (SEM/EDX)

SEM (QUANTA FEG 250 microscope) was conducted to elucidate the surface morphology of the samples with the combination of EDX to aid in the detection of potential changes that may have occurred following the complexation process. PPN, MAS or the complex was mounted on a metal stub with double-sided adhesive tape and sputter coated with a thin layer of gold. The micrographs of the samples studied were taken at various magnifications at 20 kV.

2.2.2.3. Differential scanning calorimetry (DSC)

1-10 mg of PPN, MAS or the complex was placed onto a 40 µL aluminium crucible with the lid hermetically sealed and heated between 25 and 500 °C, at a rate of 10 °C/min using a DSC instrument running under nitrogen gas (Mettler Toledo, Switzerland).

2.2.2.4. X-ray powder diffraction (XRPD)

Analysis of the PPN, MAS and complex was performed at an angular range 2.5 - 70° (2θ) and a step angle of 0.02 ° (2θ) s^{-1} using a D2 PHASER (BRUKER). The X-ray source was generated as a Cu radiation at 30 kV and 10 mA.

2.2.2.5. Small angle X-ray scattering (SAXS)

Small Angle X-Ray Scattering (SAXS) was used to study the morphological changes of MAS upon the formation of flocculates following the adsorption of PPN onto MAS. The SAXS intensity is determined as a function of the scattering vector:

$$I(q) = N_p(1/q) \times n_e^2(1/q) \qquad \text{Equation 4}$$

where $N_p(1/q)$ is the number of scattering elements in the exposed volume, and $n_e^2(1/q)$ is the square of the electron number in the exposed volume (Odo et al., 2015). The scattering vector is given by the following equation:

$$q = 4\pi sin(\Theta/2)/\lambda \quad \text{Equation 5}$$

where Θ is the scattering angle and λ is the X-ray beam wavelength.

Two-dimensional (2D-SAXS) measurements on MAS and the flocculated complexes prepared were performed on a Nanostar system (Bruker, Germany). Cu Kα radiation (λ = 01542 nm) was produced to by a microfocus X-ray generator which generated a parallel X-ray beam, having an approximate 0.9 mm diameter spot size. The entire beam path was evacuated to minimise the scattering of air. The power setting used was 50.0 kV and 600 µA and sample to detector distance was 1.0765 m. The sensitivity of the detector was calibrated using a silver behenate reference standard.

Solid-state analysis: MAS and double drug loaded complexes (particle size 63-125 µm), as prepared and described in *section 2.2.1*, were placed in disposable borosilicate glass capillary tubes (diameter 2.0 mm) and sealed at both ends (Figure 2). 2D-SAXS patterns were collected for all the samples and for the background using an acquisition time of 1000 sec. Transmission was also calculated using a glassy carbon filter to correct for the probability of sample absorption using Equation 6.

$$t = \frac{I_{X+GC} - t_{GC}.I_X}{I_{GC} - t_{GC}.I_0} \quad \text{Equation 6.}$$

where t_{GC} is glassy carbon filter transmission, I_X is the number of counts collected from sample, I_{X+GC} is the number of counts from sample with glassy carbon filter, I_{GC} is the number of counts with glassy carbon filter and I_0 is the number of counts from empty chamber.

Liquid-state analysis: MAS and 1:1 v/v MAS-drug complex dispersions were prepared using a MAS dispersion concentration of 0.25 % w/v. MAS dispersion and flocculated MAS-drug complexes were collected using a micropipette and placed in a metal cell fitted with a glass capillary (Figure 2d), having a 1 mm diameter. Nanography was used to determine the coordinates of the sample holder. Data acquisition time was 1000 s and the background scattering (i.e. ultra-pure water at pH 5) was subtracted from each sample prior to data analysis.

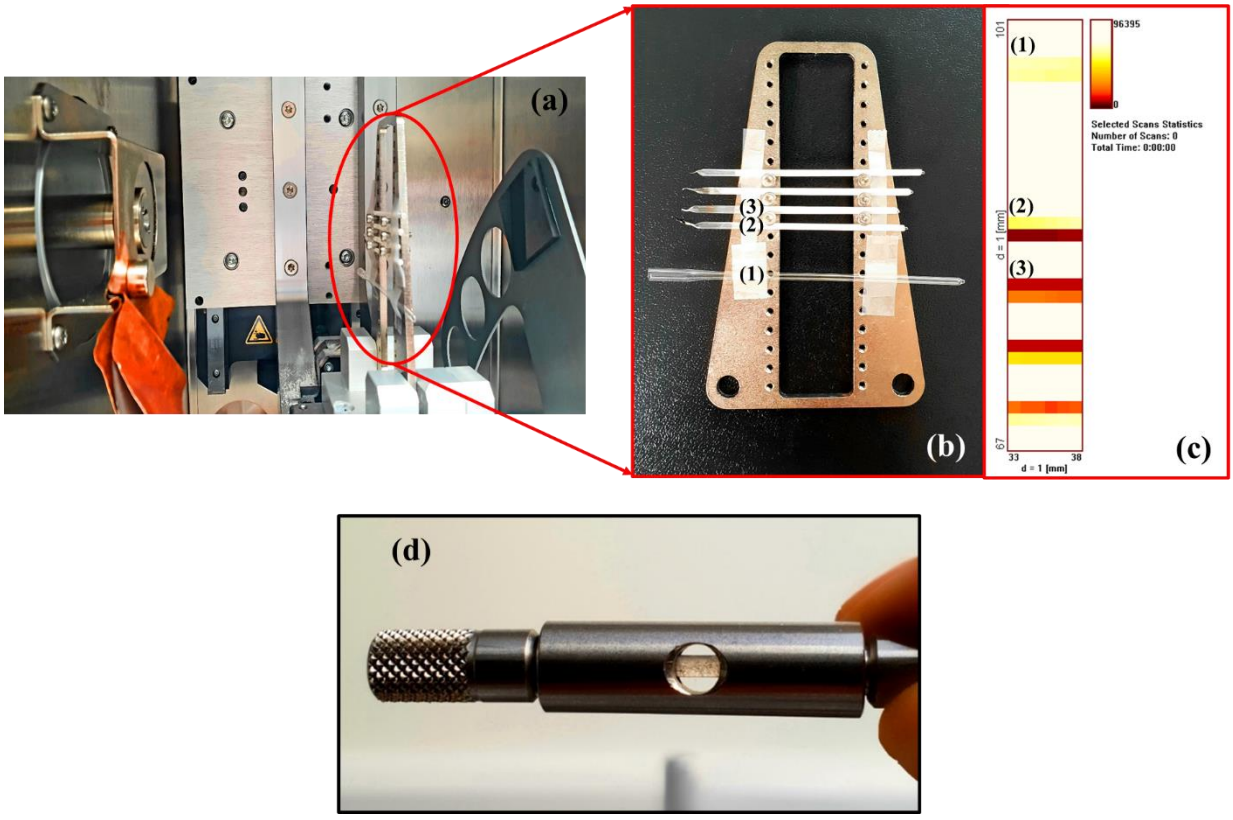

Figure 2. SAXS analysis setup showing: (a) Nanostar chamber with the sample holder, (b) sample holder image showing empty borosilicate glass capillary tube (1) and filled capillary tubes with MAS (2) and MAS-PPN (3)in powder form, particle size 63 – 125 µm, (c) nanography to detect sample coordinates for the analysis showing capillaries (1) to (3), (d) SAXS analysis setup showing MAS-drug flocculated complex dispersion placed into a metal cell fitted with a glass capillary sealed at both ends (1 mm diameter)

235 *2.2.3. Drug content analysis from the MAS-PPN complexes using HPLC*

236 Drug content within the MAS-PPN complexes was determined by dispersing 50 mg of the
237 prepared complex particles in 100 mL of a 2 M HCl, ultra–pure water or pH 6.8 phosphate
238 buffer under continuous stirring for 24 h, at 25 ºC and 700 rpm and filtered using 0.2 µm syringe
239 filters. The clear supernatant was analysed using reversed phase high performance liquid
240 chromatography (Shimadzu HPLC, Japan), equipped with an SPD-20AV UV-Vis detector,
241 using an XTerra® MS C18 150 mm × 4.6 mm × 3.5 µm column. The mobile phase was prepared
242 using acetonitrile and 0.01 M sodium phosphate dibasic dihydrate (pH 3.5) at a ratio of 30:70
243 v/v. The flow rate of the mobile phase was set at 1 mL/min with a detection wavelength of 230
244 nm.

245

246 *2.4. Tablet preparation and bulk compaction behaviour*

247 The powder mixture required to make the tablets containing MAS-drug complex was prepared
248 by mixing the amount of MAS-PPN complex equivalent to a set amount of active ingredient
249 (i.e. 40 mg PPN) with PEO at a ratio of 1:1 w/w. The powder mixture required to make the
250 tablets containing MAS-drug physical mixture and PEO was prepared using the same amounts
251 of powder as in the tablets containing MAS-drug complex particles (equivalent to a set amount
252 of active ingredient) (Table 1). The powder combination was mixed in a 3-D shaker/mixer
253 Turbula T2F (Stort Eskens Ltd., UK) for 10 min. No diluent was therefore used within the
254 matrices, hence, the compacts had different weights. The powder mixture was poured into the
255 die and tablets were formed by applying a set force of 10 kN. A pre-set maximum force was
256 set at 16 kN. During the compression stage, the displacement was measured accurately through
257 a short-travel extensometer by the movement of the cross head of the machine which was set
258 at 3 mm min^{-1} while the lower punch remained fixed. After the set force was reached, the upper-

punch was allowed to retract at a speed of 1 mm min^{-1}. Force and displacement as functions of time (F(t), respectively x(t)) were recorded automatically during the experiments. The recorded displacement was corrected using the apparent displacement under load of the instrument that was determined by performing compaction as described above on the empty die. Once the process finished and the force applied returned to zero, the specimens were ejected from the die using the same instrument set at a speed of 10 mm/min. The weight, as well as diameter and height of the specimens were recorded immediately.

The effects of compaction force on the materials used was studied as the average pressure across the upper punch P(t) vs. the relative density of the compacted samples (ρ_{rel}) (Equations 7 and 8) (Laity et al., 2015).

$$P(t) = F(t)/\pi R^2 \quad \text{Equation 7}$$

$$\rho_{rel}(t) = \frac{m}{\rho\pi R^2[h_0 - x(t)]} \quad \text{Equation 8}$$

where h_0 is the filling depth of the powder bed and m is the mass of the tablet measured after ejection from dye. Results were compared in each case between tablets containing MAS-drug complexes and tablets containing MAS-drug physical mixture.

Table 1. Formulation codes for tablets prepared using MAS-PPN complexes or MAS-PPN physical mixture (both containing an equivalent of 30 mg PPN), and PEO in different amounts (50 %, 30 %, 10 % and 5 % w/w) and their powder and compact properties (n = 3).

Formulation	**Polymer amount in formulation (% w/w)**	***Formulation code***	**True density (kg/m^3)**	**Relative density** Uncompacted	At maximum pressure	After ejection	**Elastic recovery (%)**	**Porosity (%)**
MAS-PPN (phys. mix) + PEO	5	*PEO5%_PM*	1945.93 ± 1.45	0.37 ± 0.00	0.83 ± 0.01	0.75 ± 0.01	9.10 ± 1.14	18.37 ± 1.20
	10	*PEO10%_PM*	1880.35 ± 5.78	0.36 ± 0.01	0.81 ± 0.02	0.73 ± 0.01	9.18 ± 0.48	16.07 ± 0.62

	30	*PEO30%_PM*	1673.43 ± 2.99	0.42 ± 0.01	0.88 ± 0.00	0.83 ± 0.01	6.38 ± 0.13	11.84 ± 0.49
	50	*PEO50%_PM*	1507.83 ± 1.86	0.44 ± 0.01	0.92 ± 0.00	0.86 ± 0.00	6.17 ± 0.48	7.89 ± 0.44
MAS-PPN (complex) + PEO	5	*PEO5%_C*	1990.50 ± 22.71	0.35 ± 0.01	0.80 ± 0.00	0.75 ± 0.01	6.99 ± 0.54	22.50 ± 0.55
	10	*PEO10%_C*	1925.27 ± 3.92	0.35 ± 0.01	0.79 ± 0.00	0.75 ± 0.01	5.95 ± 0.78	20.19 ± 0.31
	30	*PEO30%_C*	1742.86 ± 12.38	0.40 ± 0.00	0.87 ± 0.00	0.83 ± 0.00	5.18 ± 0.27	12.64 ± 0.29
	50	*PEO50%_C*	1515.72 ± 2.22	0.47 ± 0.00	0.85 ± 0.00	0.81 ± 0.00	4.23 ± 0.25	8.43 ± 0.96

2.4.1. True density and porosity determination

The true density of the powder mixtures used to make tablets was determined by helium pycnometry on an AccuPyc II 1340 (Micrometrics, UK). The determination of the true density of the formulations (Table 1), along with the tablet weight, height and diameter allowed for the determination of tablet porosity (Equation 9).

$$Tablet\ porosity = \left[1 - \frac{Tablet\ weight/Tablet\ \ volume}{True\ density\ of\ powder}\right] x100 \qquad \text{Equation 9}$$

Cohesive strength of the tablets prepared (σ_C) was measured based on the maximum force required for diametral crushing (F_C) (hardness of the tablets) using Equation 10.

$$\sigma_C = \frac{F_C}{\pi R_S h_S} \qquad \text{Equation 10}$$

where R_s and h_S represent the radius and the height of the tablet immediately before crushing.

2.5. Dissolution testing

The *in vitro* release characteristics of the tablets prepared were analysed using a USP dissolution apparatus with sinkers (paddle method; PT-DT70 Pharma Test, Germany). Tablets

were tested in 900 mL of 0.1 M hydrochloric acid (pH 1.2) to simulate the gastric fluid for up to 9 h or 900 mL of phosphate buffer (pH 6.8) to simulate the intestinal fluid for up to 9 h. The rotation speed of the paddles was 100 rpm. Samples were collected automatically at suitable intervals and analysed at a wavelength of 290 nm in each case by the UV-Vis detector attached to the dissolution instrument. All experiments were performed in triplicate for reproducibility.

2.5.1. Kinetics of drug release and dissolution parameters

The dissolution profiles obtained were described by the Peppas model also known as power law and was used to determine the release mechanism based on the value of the diffusional exponent (Equation 11) (Dash et al., 2010; Siahi-Shadbad et al., 2011; Romero et al., 2018).

$$Q = kt^n \qquad \text{Equation 11}$$

where Q is the percentage of drug released at time t, k is the release rate constant which describes the structure and geometry of the tablet, and n is the diffusional exponent which indicated the mechanism of drug release (Dash et al., 2010; Siahi-Shadbad et al., 2011; Romero et al., 2018). A value of n lower than 0.45 calculated from drug release of cylindrical tablets indicates a Fickian diffusion mechanism. A value of n higher than 0.89 shows that the dissolution process was controlled by erosion and that the rate of drug release was independent of time, i.e. 'zero-order' release. An anomalous transport (or non-Fickian) is considered when n was between 0.45 and 0.89 which suggests that drug release is governed by both diffusion and erosion (Ritger and Peppas, 1987; Costa, Manuel and Lobo, 2001; Siahi-Shadbad et al., 2011).

The efficiency on retarding drug release using PEO combined with both MAS-PPN complexes and physical mixtures were compared using the following equations describing the mean dissolution time (MDT) and the dissolution efficiency (DE – area under the dissolution curve

up to a certain time *t*) (Equations 12 and 13) (Costa, Manuel and Lobo, 2001; Siahi-Shadbad et al., 2011).

$$MDT = \frac{\sum_{j=1}^{n} t\Delta M_j}{\sum_{j=1}^{n} \Delta M_j} \quad \text{Equation 12}$$

where j is the sample number, n is the number of dissolution sample times, t is the time at midpoint between t and $t-1$ (that can be calculated with the formula $(t + t - 1)/2$) and ΔM_j is the additional amount of drug that dissolved between t and $t-1$ (Costa, Manuel and Lobo, 2001; Siahi-Shadbad et al., 2011).

$$DE = \frac{\int_0^T Y \times dt}{Y_{100} \times T} \times 100\% \quad \text{Equation 13}$$

where Y is the percent of drug release at time t and Y_{100} represents 100 % drug release (Costa, Manuel and Lobo, 2001; Siahi-Shadbad et al., 2011).

2.6. Calorimetric binding studies - effects of PEO on the MAS-PPN interactions

Calorimetric single and multiple injection mode (SIM and MIM) binding studies on PPN and MAS were carried out exactly as detailed in Totea et al., 2019 using a VP-ITC micro calorimeter (Malvern Panalytical, UK) to allow the determination of the association constant Ka and the thermodynamic parameters ΔH, ΔG and ΔS.

To ascertain the effects of PEO on the MAS-PPN complexes or how possible interactions between, drug, MAS and PEO could inform the choice of formulation as well as the dissolution process, calorimetric MIM binding studies were carried out on the VP-ITC instrument (calibrated to ensure the instrument was within acceptable limits (Baranauskiene *et al.*, 2009)) at pH 5 and at two different temperatures (25 °C and 37 °C). A high-gain feedback mode whilst applying a reference power of 20 μcal s^{-1} under stirring at 307 rpm was used. The real-time binding isotherm was studied in 29-120 injections of 2-10 μL each into the sample cell every

260-550 s. PEO dispersions were prepared separately using purified water under stirring at 500 rpm (25 ºC) for 24 h. Each of the prepared dispersions was separately combined with one MAS dispersion and the resultant MAS-polymer complex was used in the sample cell. Fresh drug solutions of PPN were then added into the sample cell containing the MAS-polymer complex (Table 2). All experiments were conducted in triplicate and the results analysed using Origin 7.0 (Microcal, Inc) software.

Table 2. Materials and parameters used in ITC SIM and MIM experiments (n = 3).

Cell		**Syringe**		**Number of injections**	**Injection volume (µL)**	**Spacing (sec)**	**Reference power (µcal/sec)**
Clay/ polymer	Concentration (% w/v)	**Drug/polymer**	Concentration (% w/v)				
MAS*	0.037	**PPN**	0.15	1	150	2500	20
MAS*	0.037	**PPN**	0.15	120	2	260	20
MAS	0.037	**PEO**	0.037	30	10	1500	15
PEO	0.037	**PPN**	0.15	30	10	1500	15
MAS-PEO	0.037 MAS 0.037 PEO	**PPN**	0.15	120	2	260	15

Note: * Results reported in Totea et al., 2019

3. Results and discussion

3.1. Solid state characterisation (SEM/EDX, ATR-FTIR, DSC and XRPD)

SEM/EDX confirmed MAS particles to be aggregated together with individual flakes observed on its surfaces (Figure 3a-c) with the presence of high amounts of silicon, aluminium and magnesium, as well as traces amounts of iron, calcium, sodium, titanium and potassium (Bandyopadhyay and Bose, 2013; Rapacz-Kmita et al., 2010; Pongjanyakul and Rojtanatanya, 2012; Kanjanakawinkul et al., 2013). The analysis of the MAS-PPN complex particles showed changes in the microstructural properties of the MAS to occur, which may be linked to the ability of the MAS-PPN complexes to control drug release (Rapacz-Kmita et al., 2010).

The presence of a hydroxyl group at 3625 cm^{-1} and stretching at 980 cm^{-1} were assigned to Si-OH and the Si-O-Si respectively (Rojtanatanya and Pongjanyakul, 2010). The broad O-H stretching of water residues had a peak at 3415cm^{-1} and the hydroxyl group bending of water crystallization had a sharp peak observed at 1640 cm^{-1} (Figure 3d) (Rojtanatanya and Pongjanyakul, 2010; Totea et al., 2020). Distinctive peaks occurring between 3380 and 3185 cm^{-1} for PPN were attributed to the secondary hydroxyl and amine groups within its structure whereas the aryl alkyl ether stretching was reported at 1268 cm^{-1}. The naphthalene group belonging to PPN was observed at 970 cm^{-1} (Figure 3d) (Rojtanatanya and Pongjanyakul, 2010). With regards to the MAS – PPN complexes, the peak observed as the hydroxyl stretching belonging to Si-OH became smaller and shifted to a lower wavelength of 3631 cm^{-1} (Figure 3d). The peaks attributed to the secondary hydroxyl and amine groups of the PPN completely disappeared however, the Si-O-Si stretching at 980 cm^{-1} belonging to the clay was still present. The PPN adsorption onto MAS is via hydrogen bond formation between the silanol groups of MAS with the amine and or hydroxyl groups of PPN (Rojtanatanya and Pongjanyakul, 2010).

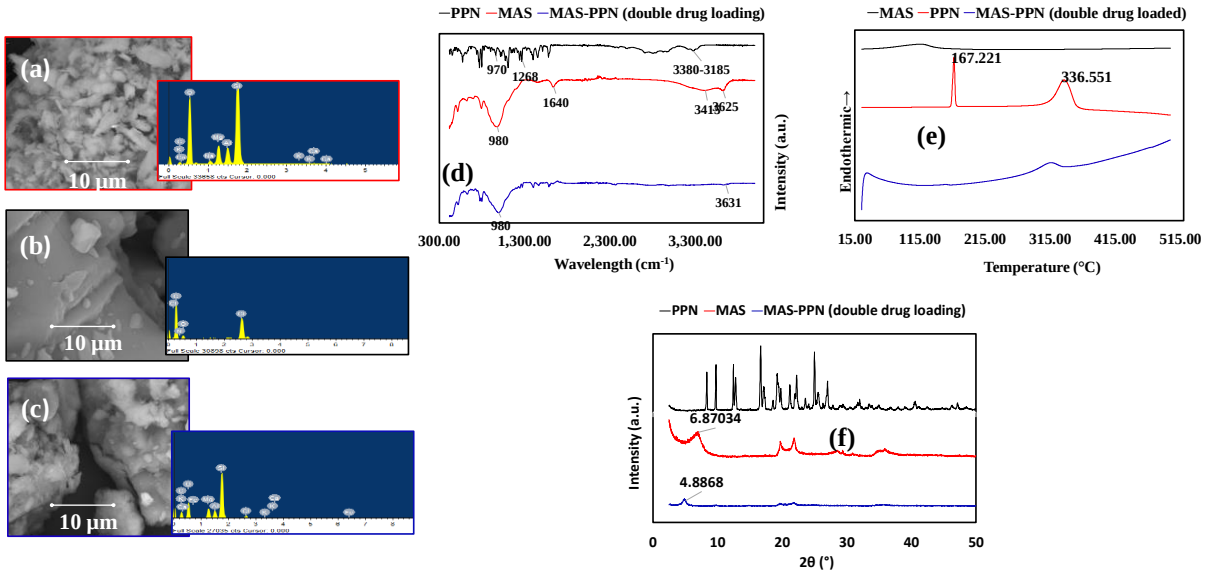

Figure 3. Solid-state analysis of the (a) SEM/EDX surface characterisation of MAS, (b) PPN, (c) MAS-PPN complex and their accompanying atomic distribution profiles (d) ATR-FTIR spectra of PPN, MAS and MAS-PPN complex particles, (e) DSC thermograph of PPN, MAS and MAS-PPN complex particles, (f) XRPD patterns for PPN, MAS and MAS-PPN complex particles

DSC thermographs were obtained for MAS, PPN and the MAS-PPN complexes to study their crystallinity. The thermograph of MAS showed the presence of a broad endothermic peak at 115 °C (Figure 3e) that occurred following dehydration, as the water residues evaporated. The thermograph of PPN revealed a sharp endothermic peak at ~ 167 °C indicating its melting point (Pongjanyakul and Rongthong, 2010; Rojtanatanya and Pongjanyakul, 2010). This was followed by another broad endothermic peak at ~ 337 °C representing the decomposition of PPN (Figure 3e). The MAS-PPN complex particles prepared were shown to be amorphous and the absence of the melting point of PPN on the thermograph confirmed that the drug was molecularly dispersed in the clay (Rojtanatanya and Pongjanyakul, 2010).

Smectite clays are often called 'expandable clays', as they have the ability to absorb water. Their typical basal spacing is 14Å (1.4nm), but following water absorption this may vary between 9.6Å (completely dried) to 21.4Å (Tucker, 2001). Basal spacing also indicates the capacity of drug molecules to intercalate into the silicate layers of the clay (Sinha et al., 2002). MAS in Figure 3f showed a distinctive reflection at 6.87034° (2θ). This was representative of the thickness of the basal spacing between platelets and was calculated using Bragg's Law (first order of reflection, n=1) as being 1.28nm, value similar to those suggested in literature (Pongjanyakul, Khunawattanakul and Puttipipatkhachorn, 2009; Rojtanatanya and Pongjanyakul, 2010). Figure 3f confirmed PPN to be crystalline in nature with strong distinctive intensities at 2-theta values at 8.3 º, 9.7 º, 12.4 º, 12.7 º, 16.7 º, 16.6 º, 17.2 º, 22.0 º and 25.0 º as previously reported (Shankland and Knight, 1996; Fernandes et al., 2019). The

prepared MAS-PPN complexes suggested the PPN drug to be molecularly dispersed within the MAS due to the absence of the crystalline peaks of PPN. The reflection at 6.87034° (2θ) representing the thickness of the silicate layer in the MAS sample was shifted to the left in the diffractogram of the complexes prepared and had a different intensity, as the basal spacing increased following intercalation of drug particles into the clay platelets, which further increased stacking of the intercalated silicate layers (Sinha et al., 2002; Rojtanatanya and Pongjanyakul, 2010). The increase in basal spacing calculated using Bragg's Law was 18.1 nm for MAS-PPN complexes (18.08 Å for MAS-PPN complexes).

3.2. Small angle X-ray scattering (SAXS)

2D-SAXS data patterns for MAS and MAS-PPN complexes were shown to be symmetric and circular, which was due to the analysis of the compounds in powder form (randomly orientated particles). The particles therefore showed no preferred orientation at the nanometre scale. The intensity plots of both MAS and MAS-PPN showing Log {I(a.u.)} vs. q [nm^{-1}] had a smooth curve, showing the intensity decreasing from $q \approx 0.099\ nm^{-1}$ (at $2\theta = 0.14^{o}$) at the edge of the beam stop, to $q = 2.275\ nm^{-1}$ (at $2\theta = 3.20^{o}$) at the peripheral limit of the detector (Figure 4). No peaks or other specific features were observed. The scattering intensity of the background was found to be minimal in comparison to the sample scattering intensity (Figure 4). The background subtraction was therefore considered unnecessary. However, data was corrected for transmission through the calculation on the transmission factor using glassy carbon. Analysis of the data in the form of a double logarithmic plot of intensity (log I [a.u.]) vs. the scattering vector (log {q [nm^{-1}]}) for both MAS and MAS-PPN complexes followed straight lines with no peaks or other specific features (Figure 4d). The straight lines indicate power-law scattering behaviour, which can be described using Equation 14.

$$I(q) = I_0 q^{-\alpha}$$ Equation 14

where I_0 and α are constants. I_0 depends on multiple factors such as collection time, incident X-ray intensity, strength of scattering etc. and α is the power-law constant that can be calculated from the slope of the linear part of the double-logarithmic plot of intensity vs. the scattering vector. A slope of – 3.63 was obtained for MAS, and a slope of – 3.57 was obtained for the MAS-PPN complex particles.

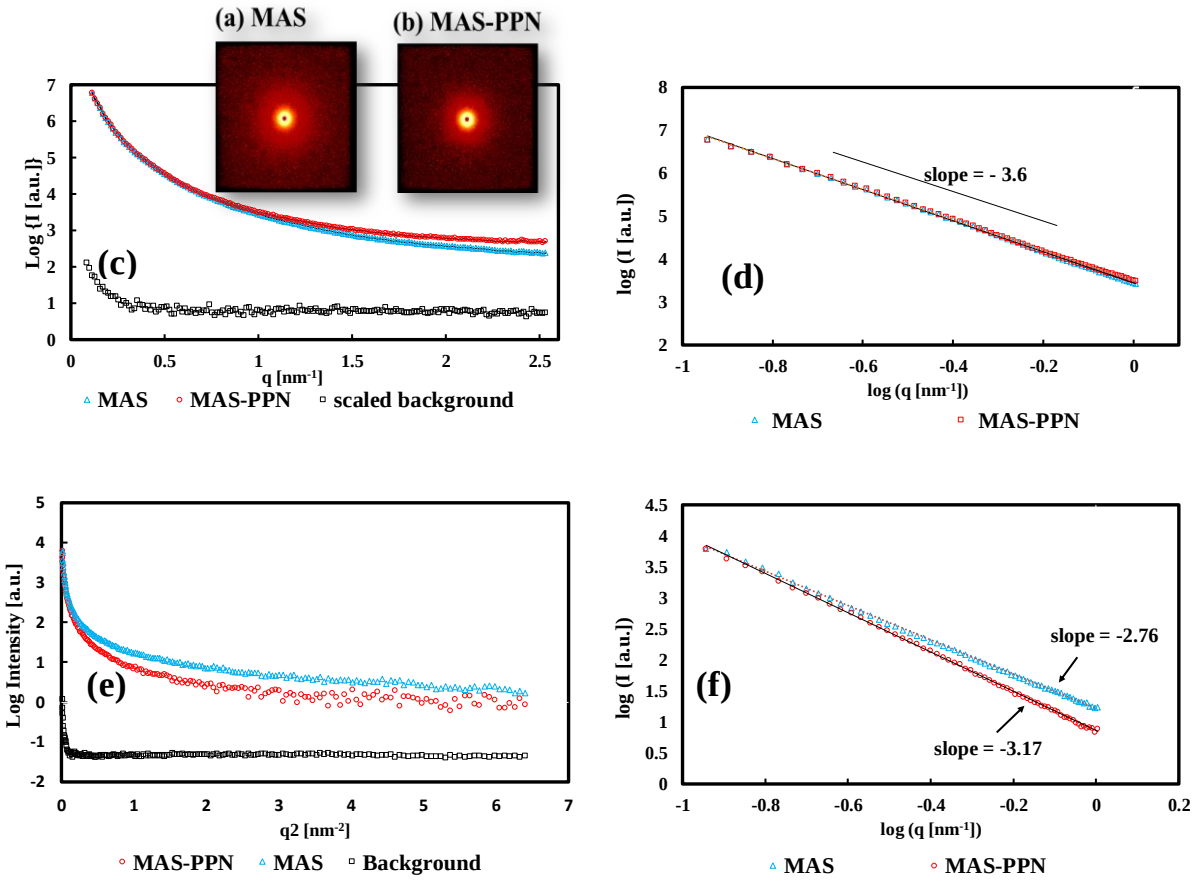

Figure 4. Typical SAXS data for samples in powder form: (a and b) 2D-SAXS patterns for MAS and MAS-PPN complexes showing the centre of the beam stop, (c) 1D-SAXS intensity curves for MAS and MAS-PPN complexes (open symbols showing uncorrected data and line showing data after scaled background subtraction), and scaled background (open black square

symbols), (d) double-logarithmic plot of intensity vs. the scattering vector for MAS and MAS-PPN complexes in powder form (particle size 63 – 125 μm), showing the slope of the linear part for the data which allows the calculation of the power-law constant a as −3.63 for MAS and −3.57 for MAS-PPN complexes, (e) Guinier plot of MAS dispersion and MAS – PPN complex dispersion showing two linear regions in the high and low q values, (f) Double-logarithmic plot of intensity vs. the scattering vector for MAS and MAS-PPN complexes in liquid form, showing power law behaviour

The value of a depends on sample morphology and allows the determination of mass and surface fractal dimensions (D_m and D_s respectively). Fractal geometry is applied to simplify the interpretation of the scattering effects from complex and disordered structures.

For mass and surface fractals the following conditions must be obeyed by α:

$\alpha = D_m$ and $0 < D_m < 3$ Equation 15

or

$\alpha = 6 - D_s$ and $2 < D_m < 3$ Equation 16

Hence, upon calculation, a surface fractal dimension value (D_s) of 2.37 and 2.43 was obtained for MAS and MAS-PPN complexes respectively, indicating that both samples tested had surface fractals over a length scale of 0.1 nm to 1.0 nm. The values obtained indicate an irregular, rough and space filling surface with the surface of MAS (D_m = 2.37) being relatively smoother compared to the surface of MAS-PPN complexes (D_m = 2.43). This may be an indication of PPN being intercalated, although this assumption however would be hard to demonstrate as other factors may contribute to slight differences between samples (such as hydration).

The α value obtained for MAS in this study was higher than that reported in a similar study showing $\alpha \approx 3$ (Laity et al., 2015). The difference in results shows a difference in structure, most probably due to the different type of MAS used (clay granules vs. fine powder used in present study) (Laity *et al.*, 2015). However, a surface fractal dimension D_s value close to the one obtained in this study was obtained for montmorillonite in a study published in 2007 by De Stefanis *et al.* (De Stefanis *et al.*, 2007). The authors used small angle neutron scattering (SANS) to determine the fractal dimension and found that montmorillonite had a surface fractal of 2.60, which implies a rough and irregular surface. Similar results were also obtained in a study published in by Pernyeszi and Dékány in 2003, where the authors reported a surface fractal dimension of 2.78 for montmorillonite using SAXS (Pernyeszi and Dékány, 2003).

Data acquired for the MAS dispersion and the flocculated complexes formed between MAS and PPN, was represented using a Guinier plot ($\log(I)$ vs. q^2). For both the MAS and the flocculated MAS-PPN complexes, the shape of the curves did not follow a linear dependence over the whole range of q. Furthermore, a careful observation of the graphs shows two linear regions separated by a transition region (Figure 4e). This behaviour suggests a poly-dispersive system in which cluster size is variable. q indicates structural characteristics, hence, the larger slope values in the higher q range compared to the lower q range indicated more scattering at higher q values (Odo *et al.*, 2015). This suggests the presence of large cluster aggregates in the samples. No peaks or other specific features were observed. Similar SAXS profiles to those obtained in this study were also reported elsewhere (Shang, James A. and Jar-shyong, 2001).

Due to the large size of clay particles which may exceed 80 nm (near the limit of the SAXS instrument), the basal distance of clays can be calculated instead of the true dimension of the particles (Shang, James A. and Jar-shyong, 2001). Using the Guinier plot, the slope of the best linear fit to the regions of lower q values allows the calculation of the radius of gyration for thickness R_g. The radius of gyration can be calculated only in the low q region because Guinier

plot is valid in the range where qR_g is lower than unity (Li, Senesi and Lee, 2016). As a consequence of the polydispersity of the MAS and MAS-PPN dispersions, the thickness R_g could not be determined accurately. The results of the thickness R_g calculated from the Guinier plot may contain high errors due to the resolution of the technique which involves the selection of a linear region (Shang, James A. and Jar-shyong, 2001). Analysis of the data in the form of double logarithmic plot of intensity (log I [a.u.]) vs. the scattering vector (log {q [nm^{-1}]}) for both MAS dispersion and MAS-PPN flocculates followed straight lines with no peaks or other specific features, indicating power-law scattering behaviour (Figure 4f). A slope of – 2.76 was obtained for MAS dispersion, while a considerably different slope of – 3.17 was obtained for the MAS-PPN complex dispersion. The difference in results shows a difference in structure, with the MAS-PPN complex dispersion having a more complex structure.

3.3. Recovery of PPN content from MAS–PPN complex particles

A higher amount of PPN was recovered from the complexes in 2 M HCl (26 % w/w) than in pH 6.8 buffer (21 % w/w) suggesting that the polydispersity of MAS particles was influenced by the cations present in the dissolution media (Rojtanatanya and Pongjanyakul, 2010). There was no PPN degradation observed in the media used for the recovery. This was similar to that reported by Totea et al. 2020. The same authors however reported degradation to occur for diltiazem hydrochloride hence the importance of screening for drug degradants.

3.4. Bulk compaction study and porosity

The true powder density was similar for the formulations containing MAS-PPN complexes and those containing MAS-PPN physical mixture which was expected as the MAS and the MAS-PPN complex particles were sieved to the same particle size fraction between 63-125 µm

(Table 1). An increase in powder density was however observed upon a decrease in polymer content in the formulations (Table 1).

Each of the tablets prepared contained an equivalent of 40 mg PPN. The amount of MAS-PPN complex that contained 40 mg PPN was calculated using the assay. Bulk compaction behaviour was studied for the formulations prepared as plots of relative density vs. upper punch pressure measured during loading to 130 MPa (10 kN) and unloading. The compaction curves of all the samples tested followed similar trends: the compaction behaviour was dominated by plastic recovery during the loading stage following non-reversible deformation, movement and fragmentation of the particles (Laity and Cameron, 2008; Laity *et al.*, 2015). Following unloading, all the specimens exhibited significant elastic recovery showing reversible deformation of some of the structures in the tablets. Overall, the elastic recovery was considerably higher for the specimens containing MAS-PPN physical mixture compared with those containing MAS-PPN complexes (Table 1). An overall increase in elastic recovery during unloading was also observed upon the decrease of polymeric content in the tablets, suggesting that the MAS in the samples exhibits significant elastic recovery upon compaction. This behaviour was previously reported in literature by Laity *et al.* (Laity *et al.*, 2015). The authors found that MAS exhibited significant elastic recovery upon compaction to 204 and 611 MPa. This behaviour was attributed to changes in the basal spacing of the clay upon compaction or to the bending of the clay platelets. The reduction in elastic recovery during compaction upon use of MAS-PPN complexes in the tablets instead of MAS-PPN physical mixture is of high importance because it reduces the chances of tablets cracking or tooling wear (Laity *et al.*, 2015). Tablet porosity was shown to be slightly higher for the tablets containing the MAS-PPN complexes (Table 1) which may offer additional benefits in controlling PPN release due to potential differences in water ingress. It is however important to also note that other important tablet characteristics such as drug solubility, surface area and particle size can influence

529 dissolution rates (Riippi *et al.*, 1998). It was also interesting to note that there was a significant
530 reduction in the porosity of the tablets with an increase in the polymer content. PEO5%_PM
531 had a porosity of 23 % and this was significantly reduced to 8 % in the PEO50%_PM tablets
532 (Table 1).

533 *3.5. Dissolution, dissolution parameters and kinetics of drug release*

534 Figure 5a-h displays the dissolution profiles of the MAS-PPN physical mixtures in comparison
535 to their complexed counterparts at the various polymers levels (5-50 %). These figures also
536 show the influence of pH media (pH 1.2 and 6.8) on these matrices. Table 3 also depicts the
537 mechanisms and kinetic values of drug release from these matrices. Matrices containing 5 %
538 polymer content with the MAS-PPN physical mixture gave sustained PPN release after an
539 initial burst in both acid and buffer. However, this behaviour was not observed in the
540 dissolution profiles of tablets containing 5 % PEO and MAS-PPN complexes which, in turn,
541 demonstrate the efficacy of the MAS-PPN reservoirs in retarding drug release (Figure 5 a and
542 b). A similar behaviour was also observed at the 10 % polymer level. These effects were
543 however less noticeable as the amount of polymer in the tablets increased to 30 % and 50 %.
544 The increase in drug release in acid compared to the buffer may also be explained by the
545 hydrogen ions having a smaller size when compared with sodium ions (28 pm compared with
546 161 pm respectively), which may promote a deeper diffusion of the hydrogen ions inside the
547 particles) (Rojtanatanya and Pongjanyakul, 2010). Furthermore, the increase in ionic strength
548 of the medium (pH 6.8) causes the polymer to lose its water hydration properties and show a
549 lower degree of swelling as ions present in solution compete for the available water of
550 hydration (Kavanagh and Corrigan, 2004). Of interest in Table 3 is the mean dissolution time
551 (MDT) values. There was an increase in the MDT values with an increase in the polymer
552 content in both media. It was also observed that the MDT values were significantly increased
553 in the pH 6.8 media with the MAS-PPN complexes having significantly higher values in all

554 cases (Table 3). The ability of the MAS-PPN complexes to control drug release is poignant
555 especially at the lower polymer levels (MDT at pH 1.2; = ~50 min and ~135 min for the
556 physical mixture and complexes respectively at the 5 % polymer level; MDT at pH 6.8; = ~92
557 min and ~169 min for the physical mixture and complexes respectively at the 5 % polymer
558 level; MDT at pH 1.2; = ~129 min and ~182 min for the physical mixture and complexes
559 respectively at the 10 % polymer level; MDT at pH 6.8; = ~138 min and ~201 min for the
560 physical mixture and complexes respectively at the 10 % polymer level (Table 3)). This
561 decrease in drug release with an increase in PEO content has also been observed previously
562 with particle size and viscosity being shown to also be a contributory factor (Shojaee et al.,
563 2013, 2015).

564 The kinetics of drug release revealed that all but one of the profiles for the physical mixture
565 formulation exhibited anomalous transport. There was a general increase in the *n* values with
566 an increase in polymer content suggesting an increase in erosion occurring with increase
567 polymer content (Table 3). There was also a general decrease in the *n* values in pH 6.8
568 compared to the pH 1.2 media. The complexes however displayed significant *n* values
569 compared to their physical mixture counterparts in both media tested. The complexes all
570 exhibited either anomalous transport or case II transport (Table 3). The case II transport kinetics
571 were observed with the significant increased polymer contents (50 % PEO contents). A
572 comparison of the physical mixture kinetics (pH 1.2 at 50 % polymer level; $n = 0.8$; pH 6.8 at
573 50 % polymer level; $n = 0.77$) and complexes (pH 1.2 at 50 % polymer level; $n = 1.06$; pH 6.8
574 at 50 % polymer level; $n = 1.07$) exhibits the importance of using the complexes in
575 manipulating drug release and its kinetics which are of importance to a formulator.

576

577

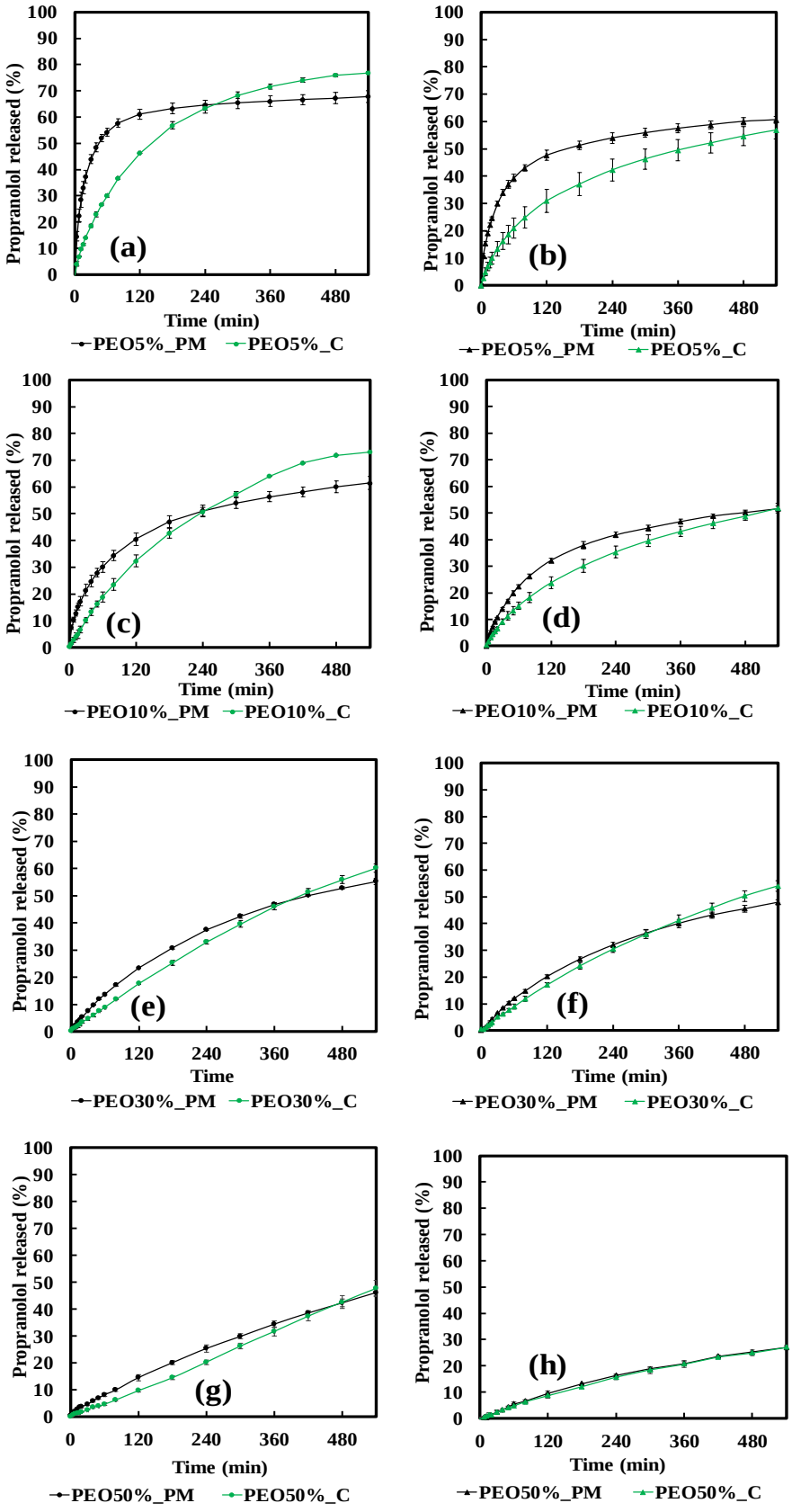

578

579 Figure 5: PPN release profile from matrices made of MAS-PPN physical mixture and complex

580 particles combined with PEO at (a) 5 % in pH 1.2, (b) 5 % in pH 6.8, (c) 10 % in pH 1.2, (d)

581 10 % in pH 6.8, (e) 30 % in pH 1.2, (f) 30 % in pH 6.8, (g) 50 % in pH 1.2, (h) 50 % in pH 6.8
582 over 9 h

583 Table 3. Mechanism and kinetics of drug release of tablet matrices prepared using MAS-PPN
584 physical mixture and MAS-PPN complexes incorporated in 5 - 50 % PEO polymer content (n
585 = 3).

Formulation	**Dissolution media**	**Polymer amount in formulation (% w/w)**	***Formulation code***	**$DE_{540\ min}$ (%)**	**MDT (min)**	***n* value**
MAS-PPN (phys. mix) + PEO	**pH 1.2**	5	*PEO5%_PM*	62.34	50.31	0.45
		10	*PEO10%_PM*	49.57	129.24	0.45
		30	*PEO30%_PM*	38.22	200.16	0.70
		50	*PEO50%_PM*	28.47	256.99	0.80
MAS-PPN (complex) + PEO	**pH 1.2**	5	*PEO5%_C*	60.57	134.75	0.70
		10	*PEO10%_C*	51.77	182.28	0.83
		30	*PEO30%_C*	37.04	254.06	0.91
		50	*PEO50%_C*	26.12	300.55	1.06
MAS-PPN (phys. mix) + PEO	**pH 6.8**	5	*PEO5%_PM*	52.44	91.58	0.35
		10	*PEO10%_PM*	40.49	137.84	0.51
		30	*PEO30%_PM*	32.89	204.26	0.68
		50	*PEO50%_PM*	25.33	254.5	0.77
MAS-PPN (complex) + PEO	**pH 6.8**	5	*PEO5%_C*	42.26	169.13	0.55
		10	*PEO10%_C*	36.23	201.2	0.63

	30	*PEO30%_C*	33.67	249.41	0.83
	50	*PEO50%_C*	21.33	291.03	1.07

586

587

588 *3.6. Calorimetric binding studies*

589 SIM and MIM studies for MAS-PPN complexes have been explored and reported previously
590 by Totea et al. 2019. The binding between MAS and PPN was reported to be predominantly
591 enthalpically driven, a consequence of changes in hydrogen bonds and electrostatic
592 interactions. Here, the authors focus on the potential interactions at the molecular level
593 between, MAS and PEO, PEO and MAS and the adsorption of PPN on MAS-PEO complexes.

594 The calorimetric signal, and therefore thermodynamic interaction between MAS and PEO at
595 25 and 37 °C differed from one another. Figure 6a suggest that PEO can weakly bind to MAS,
596 as expected based on previously reported findings (Gao, 2004). The binding isotherm at 25 °C
597 (Figure 6a) indicates endothermic, non-constant heats in the later stages of the titration in the
598 presence of excess PEO. This could be a consequence of the aggregation of PEO-MAS
599 complexes or a contribution of the PEO or MAS self-aggregation in water at pH 5. Aggregation
600 is known to be a rather random and somewhat unpredictable process that can contribute to the
601 experimental heat measured by the calorimeter and compete with the binding process
602 (Velazquez-Campoy and Freire, 2006). An increase in temperature was shown to reduce the
603 occurrence of aggregation, as evidenced by the comparatively constant ITC heat signals in the
604 later stages of MAS titration with excess PEO at 37 °C (Figure 6b). A further investigation of
605 PEO dilution into water at pH 5 (25 °C) displayed a monotonous decrease of ITC heat signals
606 without sigmoidal behaviour, suggesting that PEO self-associates weakly in aqueous solution.
607 This finding fits well with a previously published study that found PEO aggregates coexist with

PEO unimers in aqueous solution (Dai and Tam, 2005). With an amphiphilic structure (hydrophobic backbone and hydrophilic side groups), PEO may show a tendency to self-aggregate in aqueous solution, even at a low concentrations. Constant heats of dilution were observed for MAS dilution into water, showing no aggregation behaviour for MAS in water at pH 5 (25 °C) (Figure not shown). This therefore suggests that PEO can intercalate between the MAS particles and hence, a model may be proposed (Figure 6 c).

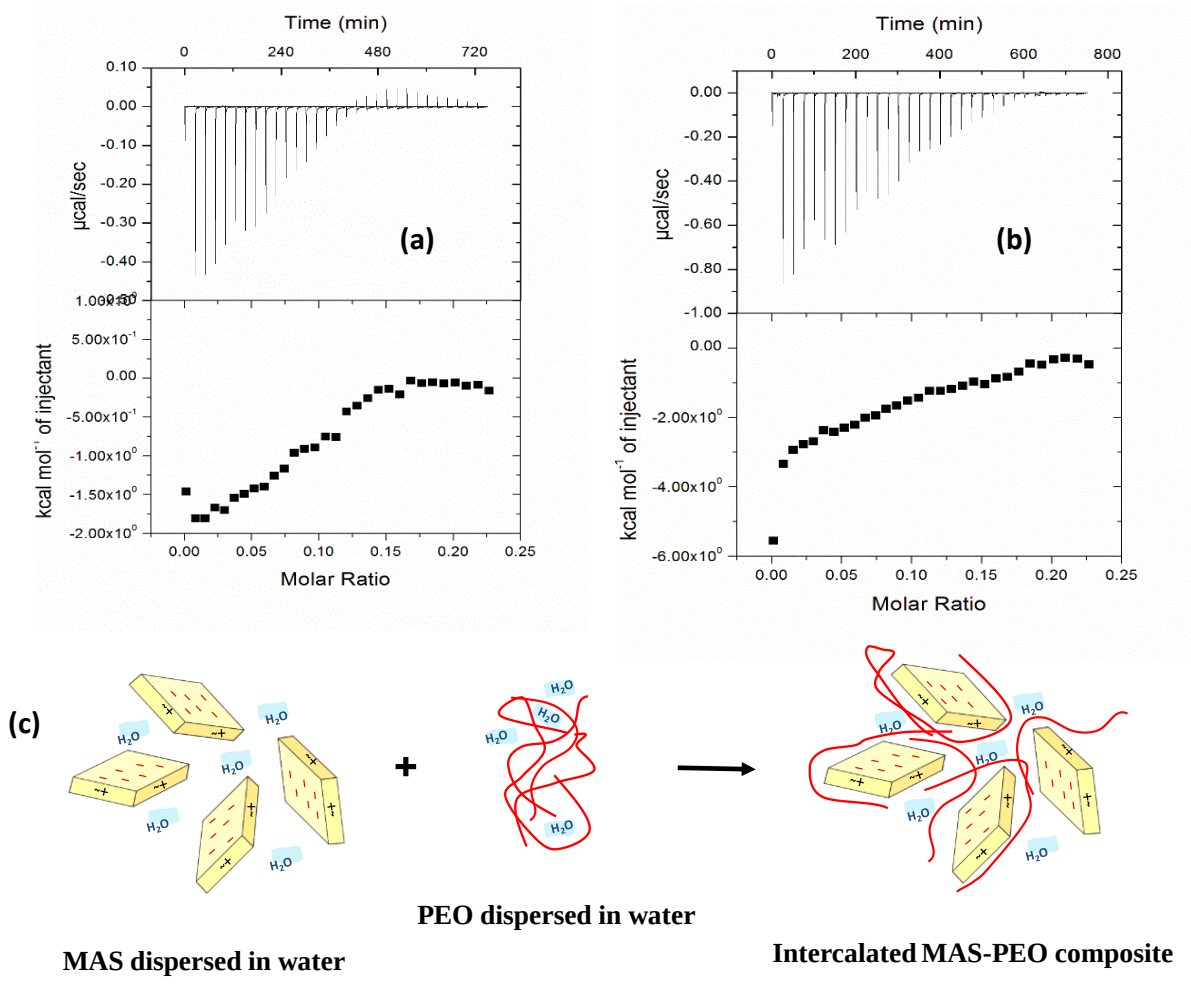

Figure 6. Titration of 0.037 % w/v PEO dispersion (pH 5) into 0.037 % w/v MAS dispersion (pH 5) at 25 °C (a) and 37 °C, (b) Raw data (top) and integrated heats (bottom) as a function of molar ratio, (c) scheme of MAS-PEO intercalated composite formation using MAS

dispersed in water and PEO dispersed in water: adapted from (Gao, 2004). Note: Red lines are PEO polymer.

Experiments conducted at pH 5 and at 25 °C showed constant dilution heats and hence no interaction occurring between PPN and PEO (Figure not shown). The same behaviour was reported previously in analysing controlled drug release through synergistic interactions between PEO and NaCMC (Palmer *et al.*, 2013).

Multiple injection stepwise experiments at pH 5 allowed the observation of the binding between PPN (0.150 % w/v) and MAS-PEO mixture (0.037 % w/v MAS; 0.037 % w/v PEO) (Figure 7a and b). The binding was highly exothermic at the two different temperatures studied (25 and 37 °C) and was characterised by a negative enthalpy change (ΔH) (-12.44 ± 0.10 kcal/mol at 25 °C and -10.68 ± 0.19 kcal/mol at 37 °C) and a positive entropy change (-TΔS) (5.99 ± 0.47 kcal/mol at 25 °C and 3.59 ± 0.23 kcal/mol at 37 °C), suggesting that the process was enthalpy driven and entropically unfavourable, as high energy resulted from broken and created hydrogen bonds as well as electrostatic van der Waals interactions. The change in temperature did not have a great impact on PPN adsorption onto MAS-PEO mixture. The change in the Gibbs free energy (ΔG) was similar for the PPN titration into MAS-PEO mixture at both temperatures (-6.46 ± 0.52 kcal/mol at 25 °C and -7.09 ± 0.18 kcal/mol at 37 °C), suggesting that both reactions occurred spontaneously (Table 4). The increase in temperature led to a slight increase in the binding affinity (K_a) between PPN and MAS-PEO mixture at 37 °C (5.37E+04 ± 7.54E+03 M at 25 °C compared to 8.63E+04 ± 6.11E+03 M at 37 °C).

Table 4. The binding parameters (affinity, free energy, binding enthalpy and entropy factor) for PPN solution (0.150 % w/v) titration into a MAS and PEO mixture (0.037 % w/v MAS; 0.037 % w/v PEO) at 25 and 37 °C (pH 5) **(n = 3)**.

	25 °C	**37 °C**

Ka (M)	5.37E+04 ± 7.54E+03	8.63E+04 ± 6.11E+03
ΔG (kcal/ mol)	-6.46 ± 0.52	-7.09 ± 0.18
ΔH (kcal/ mol)	-12.44 ± 0.10	-10.68 ± 0.19
-TΔS (kcal/ mol)	5.99 ± 0.47	3.59 ± 0.23

Differences between PPN adsorption onto MAS, compared to PPN adsorption onto MAS-PEO mixture were observed which are due to the addition of the PEO polymer to the reaction (Totea et al., 2019). At both temperatures studied the binding affinity (K_a) was greater for the titration of PPN into the MAS-PEO mixture (5.37E+04 ± 7.54E+03 M at 25 °C and 8.63E+04 ± 6.11E+03 M at 37 °C), compared with the affinity obtained upon binding between PPN and MAS (2.61E+04 ± 2.71E+03 M at 25 °C and 1.48E+04 ± 1.48E+03 M at 37 °C), suggesting a stronger binding. Studies showed no interaction between PEO and PPN. However, MAS and PEO binding was confirmed, which may imply that some of the sites available on the clay for PPN adsorption would have been saturated with PEO during the preparation of the MAS-PEO mixture prior to the injection of PPN. Hence, PEO binding onto the clay may interfere with the amount of PPN adsorbed onto MAS. This may potentially impact on PPN release from tablets made of MAS-PPN complex particles and PEO (added as a physical mixture) as the polymer may saturate available sites onto the clay preventing the drug being readsorbed once released. Based on the findings concerning the binding reactions taking place between MAS, PPN and PEO, a reaction scheme may be proposed which can explain the dissolution process observed (Figure 7 c).

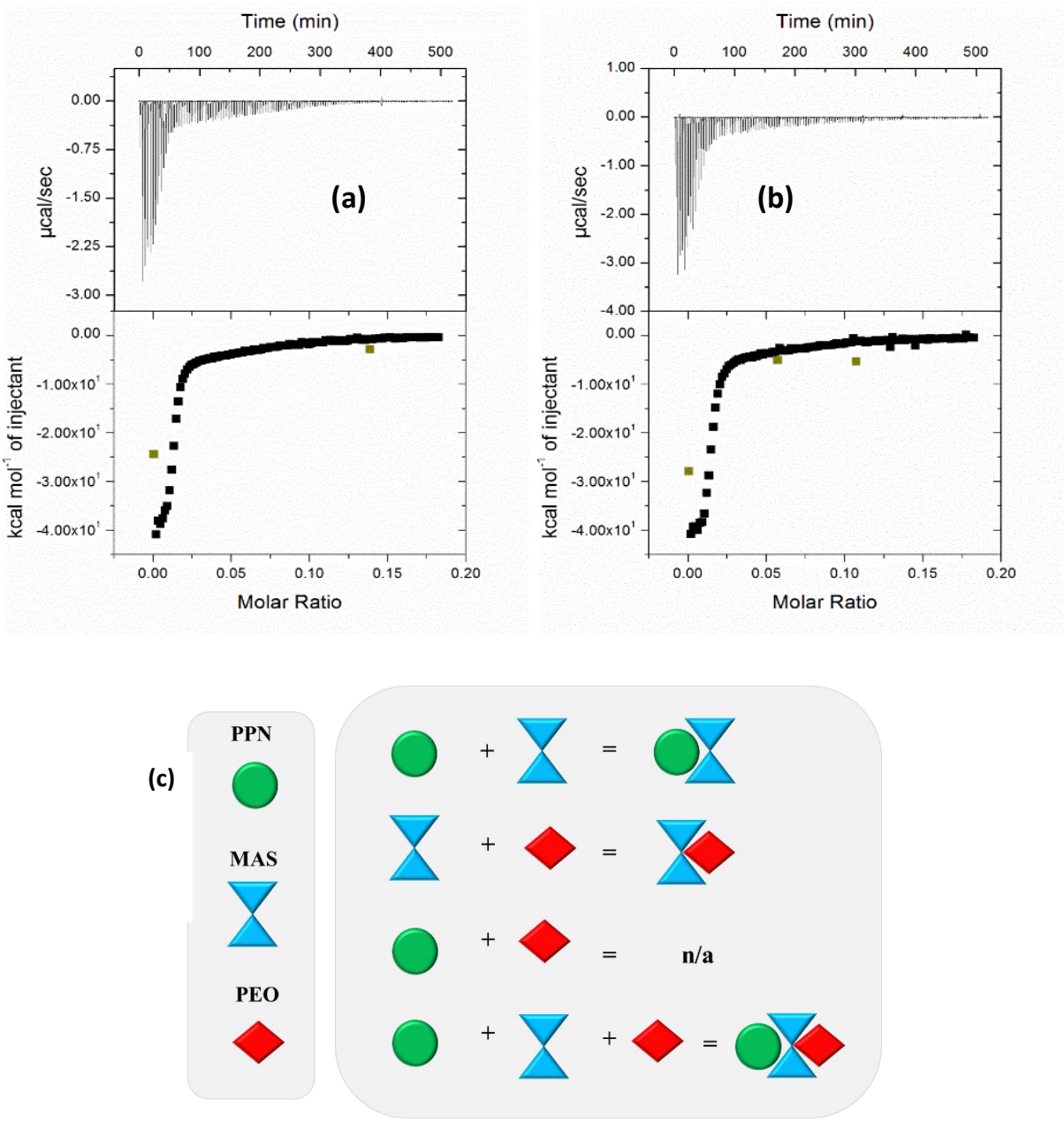

Figure 7. Titration of 0.150 % w/v PPN solution (pH 5) into MAS-PEO mixture (0.037 % w/v MAS; 0.037 % w/v PEO; pH 5) at 25 °C (a) and 37 °C (b). Results are based on three independent repeats conducted under identical conditions. Schematic representation using shapes of possible chemical interactions between PPN, MAS and PEO based on isothermal titration calorimetry results (c).

4. Conclusion

MAS-PPN flocculates were dried and characterised using a wide variety of techniques namely ATR-FTIR, PXRD, DSC, SEM/EDX, HPLC and SAXS which all confirmed changes as a result of the binding process between the two materials which may have benefits for formulators through controlled drug release. The binding between PEO and PPN and MAS was also assessed using ITC to give insights into the thermodynamics. No binding was observed between PPN and PEO, whilst PEO was shown to be adsorbed onto MAS. The influence of the PEO on the PPN adsorption onto MAS was also observed when PPN was adsorbed onto the MAS-PEO mixture. This was probably a consequence of a reduction in the available sites on MAS for binding. The thermodynamic parameters calculated suggest that the process was enthalpically driven. The compact made from the MAS-PPN complexes or MAS-PPN physically mixed with PEO revealed a compaction behaviour that was dominated by plastic recovery during the loading stage following non-reversible deformation, movement and fragmentation of the particles. Dissolution in pH 1.2 and pH 6.8 showed that PEO was able to control PPN release in both media with very low polymer concentrations in tablets (5% w/w). An increase in polymer content to up to 50 % incorporated with the MAS-PPN complexes displayed case II transport drug release meaning drug release the dissolution process was controlled by erosion and that the rate of drug release was independent of time thereby a 'zero-order' release.

5. Acknowledgements

The authors acknowledge the University of Huddersfield for funding Ana-Maria Totea.

691 **References**

692 Adebisi, A. O., Conway, B. R., & Asare-Addo, K. (2015). The influence of fillers on
693 theophylline release from clay matrices. *American Journal of Pharmacological Sciences*, *3*(5),
694 120-125.

695 Bandyopadhyay, A. and Bose, S. (eds) (2013) *Characterization of Biomaterials Chapter 4*.
696 Oxford, UK: Elsevier

697 Baranauskienė, L., Petrikaitė, V., Matulienė, J., & Matulis, D. (2009). Titration calorimetry
698 standards and the precision of isothermal titration calorimetry data. *International journal of*
699 *molecular sciences*, *10*(6), 2752-2762.

700 Callies, O., & Daranas, A. H. (2016). Application of isothermal titration calorimetry as a tool
701 to study natural product interactions. *Natural product reports*, *33*(7), 881-904.

702 Carretero, M. I., & Pozo, M. (2009). Clay and non-clay minerals in the pharmaceutical
703 industry: Part I. Excipients and medical applications. *Applied Clay Science*, *46*(1), 73-80.

704 Costa, P., & Lobo, J. M. S. (2001). Modeling and comparison of dissolution profiles. *European*
705 *journal of pharmaceutical sciences*, *13*(2), 123-133.

706 Dai, S., & Tam, K. C. (2005). Laser light scattering and isothermal titration calorimetric studies
707 of poly (ethylene oxide) aqueous solution in presence of sodium dodecyl sulfate. *Journal of*
708 *colloid and interface science*, *292*(1), 79-85.

709 Dash, S., Murthy, P. N., Nath, L., & Chowdhury, P. (2010). Kinetic modeling on drug release
710 from controlled drug delivery systems. *Acta Pol Pharm*, *67*(3), 217-23.

711 Datta, M. (2013). Clay–polymer nanocomposites as a novel drug carrier: Synthesis,
712 characterization and controlled release study of Propranolol Hydrochloride. *Applied clay*
713 *science*, *80*, 85-92.

De Stefanis, A., Tomlinson, A. A. G., Steriotis, T. A., Charalambopoulou, G. C., & Keiderling, U. (2007). Study of structural irregularities of smectite clay systems by small-angle neutron scattering and adsorption. *Applied Surface Science*, *253*(13), 5633-5639.

Fernandes, J., Celestino, M. T., Tavares, M. I., Freitas, Z. M., SANTOS, E. P., Ricci Junior, E., & Monteiro, M. S. (2019). The development and characterization of Propranolol Tablets using Tapioca starch as excipient. *Anais da Academia Brasileira de Ciências*, *91*(1).

Gao, F. (2004). Clay/polymer composites: the story. *Materials today*, *7*(11), 50-55.

Gomes, C. D. S. F. (2018). Healing and edible clays: a review of basic concepts, benefits and risks. *Environmental geochemistry and health*, *40*(5), 1739-1765.

Kavanagh, N. and Corrigan, O. I. (2004) 'Swelling and erosion properties of hydroxypropylmethylcellulose (Hypromellose) matrices - Influence of agitation rate and dissolution medium composition', *International Journal of Pharmaceutics*, 279(1–2), pp. 141–152.

Kanjanakawinkul, W., Rades, T., Puttipipatkhachorn, S., & Pongjanyakul, T. (2013). Nicotine–magnesium aluminum silicate microparticle surface modified with chitosan for mucosal delivery. *Materials Science and Engineering: C*, *33*(3), 1727-1736.

Khlibsuwan, R., & Pongjanyakul, T. (2016). Chitosan-clay matrix tablets for sustained-release drug delivery: Effect of chitosan molecular weight and lubricant. *Journal of Drug Delivery Science and Technology*, *35*, 303-313.

Khlibsuwan, R., Siepmann, F., Siepmann, J., & Pongjanyakul, T. (2017). Chitosan-clay nanocomposite microparticles for controlled drug delivery: Effects of the MAS content and TPP crosslinking. *Journal of Drug Delivery Science and Technology*, *40*, 1-10.

736 Ladbury, J. E., & Chowdhry, B. Z. (1996). Sensing the heat: the application of isothermal
737 titration calorimetry to thermodynamic studies of biomolecular interactions. *Chemistry &*
738 *biology*, *3*(10), 791-801.

739 Laity, P. R., Asare-Addo, K., Sweeney, F., Šupuk, E., & Conway, B. R. (2015). Using small-
740 angle X-ray scattering to investigate the compaction behaviour of a granulated clay. *Applied*
741 *Clay Science*, *108*, 149-164.

742 Laity, P. R., & Cameron, R. E. (2008). A small-angle X-ray scattering study of powder
743 compaction. *Powder technology*, *188*(2), 119-127.

744 Le, V. H., Buscaglia, R., Chaires, J. B., & Lewis, E. A. (2013). Modeling complex equilibria
745 in ITC experiments: thermodynamic parameters estimation for a three binding site
746 model. *Analytical biochemistry*, *434*(2), 233.

747 Li, T., Senesi, A. J., & Lee, B. (2016). Small angle X-ray scattering for nanoparticle
748 research. *Chemical reviews*, *116*(18), 11128-11180.

749 Malvern Instruments (2015) *Single Injection Method Software for MicroCal ™ VP-ITC system*.
750 Malvern.

751 MicroCal (1998) *VP-ITC User's Manual*. Northampton

752 Rapacz-Kmita, A., Krupa, A., & Jachowicz, R. (2010). Preliminary approach to application of
753 modified smectite clay to form tablets in direct compression process. *Materiały*
754 *Ceramiczne*, *62*(3), 366-368.

755 Moore, D. E., Goode, D. R., Seney, C. S., & Boatwright, J. M. (2016). Isothermal titration
756 calorimetry can provide critical thinking opportunities. *Journal of Chemical Education*, *93*(2),
757 304-310.

758 Odo, E. A., Britton, D. T., Gonfa, G. G., & Harting, M. (2015). SAXS study of silicon
759 nanocomposites. *Int. J. Compos. Mater*, *5*, 65-70.

760 Okeke, O. C., & Boateng, J. S. (2017). Nicotine stabilization in composite sodium alginate
761 based wafers and films for nicotine replacement therapy. *Carbohydrate polymers*, *155*, 78-88.

762 Okeke, O. C., & Boateng, J. S. (2016). Composite HPMC and sodium alginate based buccal
763 formulations for nicotine replacement therapy. *International journal of biological*
764 *macromolecules*, *91*, 31-44.

765 Palmer, D., Levina, M., Douroumis, D., Maniruzzaman, M., Morgan, D. J., Farrell, T. P., ... &
766 Nokhodchi, A. (2013). Mechanism of synergistic interactions and its influence on drug release
767 from extended release matrices manufactured using binary mixtures of polyethylene oxide and
768 sodium carboxymethylcellulose. *Colloids and Surfaces B: Biointerfaces*, *104*, 174-180.

769 Patrick, G. (2001) *Medicinal Chemistry*. Oxford, UK: BIOS Scientific Publishers Limited.

770 Penn, C. J., & Warren, J. G. (2009). Investigating phosphorus sorption onto kaolinite using
771 isothermal titration calorimetry. *Soil Science Society of America Journal*, *73*(2), 560-568.

772 Pernyeszi, T., & Dékány, I. (2003). Surface fractal and structural properties of layered clay
773 minerals monitored by small-angle X-ray scattering and low-temperature nitrogen adsorption
774 experiments. *Colloid and Polymer Science*, *281*(1), 73-78.

775 Pongjanyakul, T., Khunawattanakul, W., & Puttipipatkhachorn, S. (2009). Physicochemical
776 characterizations and release studies of nicotine–magnesium aluminum silicate
777 complexes. *Applied Clay Science*, *44*(3-4), 242-250.

778 Pongjanyakul, T., Priprem, A., & Puttipipatkhachorn, S. (2005). Investigation of novel
779 alginate− magnesium aluminum silicate microcomposite films for modified-release
780 tablets. *Journal of controlled release*, *107*(2), 343-356.

781 Pongjanyakul, T., Khunawattanakul, W., Strachan, C. J., Gordon, K. C., Puttipipatkhachorn,
782 S., & Rades, T. (2013). Characterization of chitosan–magnesium aluminum silicate
783 nanocomposite films for buccal delivery of nicotine. *International journal of biological*
784 *macromolecules*, *55*, 24-31.

785 Pongjanyakul, T., & Rojtanatanya, S. (2012). Use of propranolol-magnesium aluminium
786 silicate intercalated complexes as drug reservoirs in polymeric matrix tablets. *Indian journal*
787 *of pharmaceutical sciences*, *74*(4), 292.

788 Puttipipatkhachorn, S., Pongjanyakul, T., & Priprem, A. (2005). Molecular interaction in
789 alginate beads reinforced with sodium starch glycolate or magnesium aluminum silicate, and
790 their physical characteristics. *International journal of pharmaceutics*, *293*(1-2), 51-62.

791 Riippi, M., Yliruusi, J., Niskanen, T., & Kiesvaara, J. (1998). Dependence between dissolution
792 rate and porosity of compressed erythromycin acistrate tablets. *European journal of*
793 *pharmaceutics and biopharmaceutics*, *46*(2), 169-175.

794 Ritger, P. L., & Peppas, N. A. (1987). A simple equation for description of solute release I.
795 Fickian and non-fickian release from non-swellable devices in the form of slabs, spheres,
796 cylinders or discs. *Journal of controlled release*, *5*(1), 23-36.

797 Rojtanatanya, S., & Pongjanyakul, T. (2010). Propranolol–magnesium aluminum silicate
798 complex dispersions and particles: Characterization and factors influencing drug
799 release. *International journal of pharmaceutics*, *383*(1-2), 106-115.

800 Romero, A. I., Villegas, M., Cid, A. G., Parentis, M. L., Gonzo, E. E., & Bermúdez, J. M.
801 (2018). Validation of kinetic modeling of progesterone release from polymeric
802 membranes. *asian journal of pharmaceutical sciences*, *13*(1), 54-62.

Rongthong, T., Sungthongjeen, S., Siepmann, J., & Pongjanyakul, T. (2013). Quaternary polymethacrylate–magnesium aluminum silicate films: molecular interactions, mechanical properties and tackiness. *International journal of pharmaceutics*, *458*(1), 57-64.

Rongthong, T., Sungthongjeen, S., Siepmann, F., Siepmann, J., & Pongjanyakul, T. (2015). Quaternary polymethacrylate–magnesium aluminum silicate films: water uptake kinetics and film permeability. *International journal of pharmaceutics*, *490*(1-2), 165-172.

Rongthong, T., Sungthongjeen, S., Siepmann, F., Siepmann, J., & Pongjanyakul, T. (2020). Eudragit RL-based film coatings: How to minimize sticking and adjust drug release using MAS. *European Journal of Pharmaceutics and Biopharmaceutics*, *148*, 126-133.

Shang, C., Rice, J. A., & Lin, J. S. (2001). Thickness and surface characteristics of colloidal 2: 1 aluminosilicates using an indirect Fourier transform of small-angle X-ray scattering data. *Clays and clay minerals*, *49*(4), 277-285.

Shankland, K., & Knight, K. S. (1996). Some observations on the crystal structure of (R, S)-propranolol hydrochloride. *International journal of pharmaceutics*, *137*(2), 255-259.

Shojaee, S., Emami, P., Mahmood, A., Rowaiye, Y., Dukulay, A., Kaialy, W., ... & Nokhodchi, A. (2015). An investigation on the effect of polyethylene oxide concentration and particle size in modulating theophylline release from tablet matrices. *AAPS PharmSciTech*, *16*(6), 1281-1289.

Shojaee, S., Asare-Addo, K., Kaialy, W., Nokhodchi, A., & Cumming, I. (2013). An investigation into the stabilization of diltiazem HCl release from matrices made from aged polyox powders. *Aaps Pharmscitech*, *14*(3), 1190-1198.

Siahi-Shadbad, M. R., Asare-Addo, K., Azizian, K., Hassanzadeh, D., & Nokhodchi, A. (2011). Release behaviour of propranolol HCl from hydrophilic matrix tablets containing

826 psyllium powder in combination with hydrophilic polymers. *AAPS PharmSciTech*, *12*(4),
827 1176-1182.

828 Sinha Ray, S., Maiti, P., Okamoto, M., Yamada, K., & Ueda, K. (2002). New
829 polylactide/layered silicate nanocomposites. 1. Preparation, characterization, and
830 properties. *Macromolecules*, *35*(8), 3104-3110.

831 Sinko, P. J. (2010) 'Pharmaceutical polymers', in *Martin's Physical Pharmacy and*
832 *Pharmaceutical Sciences*, pp. 492–515

833 Totea, A. M., Dorin, I., Gavrilov, G., Laity, P. R., Conway, B. R., Waters, L., & Asare-Addo,
834 K. (2019). Real time calorimetric characterisation of clay–drug complex dispersions and
835 particles. *International journal of pharmaceutics: X*, *1*, 100003.

836 Totea, A. M., Sabin, J., Dorin, I., Hemming, K., Laity, P. R., Conway, B. R., ... & Asare-Addo,
837 K. (2020). Thermodynamics of clay–drug complex dispersions: Isothermal titration
838 calorimetry and high-performance liquid chromatography. *Journal of Pharmaceutical*
839 *Analysis*, *10*(1), 78-85.

840 Tucker, M. E. (2001) *Sedimentary Petrology: An Introduction to the Origin of Sedimentary*
841 *Rocks*. 3rd edn. United Kingdom: Blackwell Publishing.

842 Vanderbilt Minerals (2014a) *VEEGUM / VAN GEL Magnesium Aluminum Silicate Magnesium*
843 *Aluminum Silicate ® The Story*. Norwalk.

844 Vanderbilt Minerals (2014b) 'VEEGUM ® Magnesium Aluminum Silicate VANATURAL ®
845 Bentonite Clay For Personal Care and Pharmaceuticals What They Are', pp. 1–27.

846 Velazquez-Campoy, A., & Freire, E. (2006). Isothermal titration calorimetry to determine
847 association constants for high-affinity ligands. *Nature protocols*, *1*(1), 186-191.

848